Comparison of Quantitative High-definition Microvessel Imaging and Shear Wave Elastography in Preoperative Prediction of Axillary Lymph Node Breast Cancer Metastasis

Setayesh Sotoudehnia
Mayo Clinic College of Medicine and Science
Soroosh Sabeti
Mayo Clinic College of Medicine and Science
David Rosen
Mayo Clinic College of Medicine and Science
Robert Fazzio
Mayo Clinic College of Medicine and Science
Nicholas B. Larson
Mayo Clinic College of Medicine and Science
Mostafa Fatemi
Mayo Clinic College of Medicine and Science
Azra Alizad (Alizad.azra@mayo.edu)
Mayo Clinic College of Medicine and Science

Research Article

Keywords: breast cancer, ultrasound microvessel imaging, axillary lymph node metastasis, flow imaging, shear wave elastography, vessel morphological biomarkers

Posted Date: January 25th, 2024

DOI: https://doi.org/10.21203/rs.3.rs-3879688/v1

Additional Declarations: No competing interests reported.

Abstract

Background

Accurate assessment of axillary lymph nodes (ALNs) is a critical step for timely diagnosis of metastasis and proper subsequent intervention in breast cancer patients. Herein, we compare the diagnostic utility of quantitative high-definition microvasculature imaging (qHDMI), shear wave elastography (SWE) and their combination for differentiation of metastatic ALNs from reactive.

Methods

A total of 85 female patients with suspicious ALNs recommended for fine needle aspiration biopsy (FNAB) were included in the study, and the pathology results were used as the gold standard for labeling the status of each ALN. Three SWE metrics and ten qHDMI-derived biomarkers were used in our analyses. Additionally, age, as well as clinical ultrasound features such as nodal size and cortical thickness were included as clinical factors. The Wilcoxon rank-sum test was utilized to analyze distributional differences in biomarkers between metastatic and reactive ALNs. Multiple elastic-net logistic regression models were developed based on varying combinations of clinical, qHDMI, and SWE feature sets. A 70%/30% train/test split was adopted, and ROC curve analyses were performed to evaluate and compare classification performance. Moreover, distributional differences in qHDMI and SWE biomarkers between ALNs corresponding to breast cancer immunohistochemical subtypes luminal A and B were investigated.

Results

Of the total of 85 ALNs included in the analysis, 42 were metastatic. Statistically significant (p-value < 0.05) differences were observed in all but one of the qHDMI biomarkers, as well as all the SWE metrics. Test-set discrimination defined by area under ROC curve (AUC) was low for the model using only clinical features (0.62; 95% CI = [0.39,0.84]), with higher performance observed for models using SWE only (0.93; [0.82,1.00]), qHDMI only (0.97; [0.91,1.00]), qHDMI-SWE (0.97; [0.92,1.00]), and qHDMI-SWE plus clinical biomarkers (0.98; [0.94,1.00]). No statistically significant improvements were seen in the combined SWE-qHDMI and SWE-qHDMI-C classification models relative to the qHDMI-only model, although power for comparison was limited. Four qHDMI biomarkers and two SWE measures exhibited statistically significant distributions among breast cancer luminal A and B subtypes.

Conclusions

qHDMI classification model was able to separate metastatic from reactive ALNs with high accuracy. qHDMI, SWE, and the combined models had improved classification performance over the baseline Clinical model. qHDMI biomarkers can be valuable in determining the malignancy status of suspicious ALNs, providing helpful information regarding breast cancer prognosis.

INTRODUCTION

Axillary lymph node (ALN) status has important predictive value for staging and prognosis in breast cancer patients [1]. Therefore, preoperative and accurate assessment of ALN status is essential for optimizing treatment strategy in patients with breast cancer. Physical examination of the axilla is extremely unreliable with limited sensitivity, resulting in about 70% false-negative and 20% false positive results [2]. Among clinical imaging modalities, digital mammography or digital breast tomosynthesis has limited value for detecting ALNs [3]. Currently, ultrasound (US) is the first-line imaging tool in assessing ALNs in recently diagnosed breast cancer, with variable sensitivity ranging from 49–87%, while the specificity ranges from 55–97% [4, 5]. Cortical thickening is a nonspecific ultrasound finding that can be seen in both reactive lymphadenopathy and nodal metastasis, leading to considerable numbers of false positives [6]. Commonly, preoperative classification of ALNs is done through US-guided biopsy, sentinel lymph node biopsy, and surgical excision that can be associated with complications including infection or long-lasting problems such as lymphedema [7–10]. A noninvasive alternative approach, therefore, is needed to accurately classify ALNs. The emergence of shear wave elastography (SWE) as a complementary tool to conventional ultrasound has relatively increased the sensitivity and specificity of ultrasound for breast cancer detection [11–15] and improved the prediction of ALN metastasis and invasiveness in breast cancer patients [16–18].

In recent years, there has been a growing interest in exploring ultrasound methods that can image angiogenesis and the formation of new blood vessels. Angiogenesis has an essential role in tumor growth and metastasis [19–21], and changes in morphological features of tumor microvessels due to angiogenic activity are positively correlated to histological grade, lymph node status, and disease prognosis [22, 23]. Thus, such structural changes in the microvessel network are expected to be important biomarkers in distinguishing metastatic ALN from reactive lymphadenopathy [24]. Evaluating the vascularity of ALNs by noninvasive techniques could be useful in predicting lymph node metastasis, especially in the absence of typical sonographic findings. Conventional Doppler ultrasound is only sensitive to fast flows, revealing patchy images of larger vessels, not structural analysis of tumor microvessels. The potential utility of superb microvascular imaging (SMI) for identifying metastatic ALN has been reported. However, the SMI technique is not based on microvessel morphology. Rather, SMI uses a vascular index, a marker derived from pixel counting [25].

Recently, a novel contrast-free ultrasound-based technique called quantitative high-definition microvasculature imaging (qHDMI) has been developed to visualize submillimeter vessels as small as 150 μm [26]. The qHDMI method uses a series of morphological filtering and vessel enhancement techniques, enabling the quantification of tumor vessel morphological parameters as quantitative HDMI biomarkers [27, 28]. This new technique has been tested for the differentiation of breast lesions [29], thyroid nodules [30], hepatic masses [31], and prediction of axillary lymph node metastasis [24]. Since both SWE and qHDMI data can be efficiently collected during the same ultrasound examination, such complementary information could be leveraged for clinical benefit.

Here we compare the performance of quantitative morphological parameters of tumor microvessels, as qHDMI biomarkers, with quantitative metrics of SWE and the combined of these two techniques. We

hypothesized that the quantitative HDMI biomarkers are independent of the elasticity parameters, and their information would complement each other for the prediction of ALN metastasis. The aim of this current study is to leverage the combined information from SWE, HDMI, and clinical parameters for the improvement of ultrasound-based diagnoses of lymph node metastasis. Toward this end, we develop a set of penalized logistic regression models that use combinations of SWE, qHDMI, and clinical parameters as predictors for biopsy-determined lymph node metastasis.

MATERIALS and METHODS

Ethics approval

This prospective study, from June 2018 to June 2023, received the institutional review board approval (IRB#13-006035 and IRB # 19-003028) and was Health Insurance Portability and Accountability Act compliant. A signed written informed consent was obtained from all participants prior to the study.

Study population

The imaging study was completed on a total of 85 women ages 18 years or older who had suspicious axillary lymph nodes identified in clinical ultrasound imaging and recommended for US-guided ALN fine needle aspiration biopsy (FNAB) as part of their clinical care plan. Patients did not receive any treatment before the study, and the pathology results of the FNAB were used as a reference gold standard. All quantitative HDMI and SWE studies were conducted prior to FNAB.

SWE

The ultrasound examinations were conducted by two sonographers with more than 35/14 and 17/12 years of US/SWE scanning experience, A GE LOGIQ E9 (LE9) clinical ultrasound machine equipped with SWE capability and a 9L-D linear array transducer (GE Healthcare, Wauwatosa, WI) was used for scanning. SWE imaging was conducted in penetration mode, allowing for deeper tissue assessment. During each acquisition, the patient was asked to hold breathing for 3 seconds to prevent motion artifacts. Sonographers were instructed to keep away from hand motion and apply minimal compression with the transducer to prevent pre-compression effect. At least six images were captured within a rectangular-shaped field of view for each lesion. Each SWE image was captured by default with a corresponding B-mode image. Three images with the fewest artifacts were selected for further processing. Using the 2D dual circle tool from the scanner, the selected region of interest (ROI) appears simultaneously on the B-mode image and the shear wave map. Up to three circular non-overlapping ROIs, 3 mm in diameter, were randomly placed on the enlarged cortex, depending on the size of the area. The mean values of the maximum, mean, and standard deviation (SD) of the shear wave velocity were calculated by the machine and converted to elasticity values in kilopascal in this study [17]. In addition to the previously mentioned metrics, we also calculated a new SWE parameter, the mass characteristic frequency (f_{mass}), and included it into our analysis as described in [32, 33]. In total, three SWE metrics, namely mean elasticity (E_{mean}), maximum elasticity (E_{max}), and f_{mass}, were included in our analysis.

HDMI

The study utilized an ALPINION E-CUBE 12R ultrasound machine (ALPINION Medical Systems, Seoul, South Korea) with the capability of plane wave imaging offering a sequence of high-frame-rate images and equipped with a linear array transducer L3-12H, operating at a frequency of 8.5 MHz. The same sonographers who did the SWE conducted ultrasound scanning for HDMI imaging. To identify the lymph nodes, we used conventional line-by-line B-mode ultrasound imaging. Subsequently, a sequence of high-frame-rate data (~ 600 frames per second) was acquired at the site of the lesion, with a total duration of 3 seconds. The acquired raw data underwent processing using the HDMI method, as described in previous studies [26, 34–36]. Our sonographers were instructed to use less preload during ultrasound examination to reduce unwanted compression on tissue microvessels. During data collection, patients were asked to remain still and hold their breath for around 3 seconds to reduce motion artifacts. For each orientation of the HDMI scanning, two acquisitions were made to improve repeatability. HDMI image processing has been done as reported in [29]. The nodes were manually segmented using B-mode images obtained from the IQ data reconstruction, and binary and skeleton images were generated to quantify morphological parameters of tumor microvessels as qHDMI biomarkers [27, 28]. These biomarkers include number of vessel segments (NV), number of branch points (NB), vessel density (VD), vessel diameter (D), distance metric as a measure of tortuosity (τ) [27], microvessel fractal dimension (FD), Murray's deviation (MD) and bifurcation angle (BA) [28]. A total of 10 HDMI biomarkers, namely NV, NB, VD, D_{max}, D_{mean}, τ_{max}, τ_{mean}, FD, MD_{max}, and BA_{max}, were included in our analysis.

Clinical ultrasound features and immunohistochemical parameters

All enrolled patients had a clinical breast and axillary lymph node imaging examination performed as part of their clinical care, and the ultrasound morphological features of lymph nodes were assessed. Among the ultrasound features of lymph nodes, cortical thickness and maximum diameter size of the lymph nodes were considered in the analysis as clinical imaging findings.

Furthermore, histologic subtype, histologic grade, estrogen receptor (ER), progesterone receptor (PR), human epidermal growth factor receptor (HER2) status, and the Ki-67 proliferative index were extracted from the breast biopsy and immunohistochemical reports and included in the final analysis.

Statistical analysis methods

The Wilcoxon rank-sum test was used to evaluate the statistical significance of the distributional differences observed in values of interest. Using the R package glmnet, elastic-net logistic regression was employed to train multivariable prediction models for lesion malignancy status. Five different models were trained and evaluated in this study. The SWE model trained on the SWE metrics, the qHDMI model trained on the qHDMI biomarkers, the qHDMI-SWE model trained on both qHDMI and SWE biomarkers, the qHDMI-SWE-C model trained on the quantitative biomarkers of HDMI and SWE, as well as three clinical features (age, maximum diameter of ALN, and ALN cortical thickness), and the Clinical model

which was trained solely on the three clinical features. The training process involved randomly selecting 70% of lesions, while the remaining 30% were reserved for model validation. Tenfold cross-validation within the training set was utilized for penalty parameter tuning, with a fixed alpha value of 0.05. Model output probabilities were then used for assessing discrimination performance in the leave-out test set via receiving operator characteristic (ROC) curves. In addition to estimating the area under the ROC curve (AUC), we evaluated the classification performance based on the Youden Index. The Youden Index, also known as the J statistic, is a common approach for determining the optimal threshold that balances sensitivity and specificity in binary classification tasks. It is calculated as the maximum value of sensitivity + specificity − 1 across all possible threshold values on the ROC curve [37]. Utilizing the Youden Index, we identified the optimal cutoff point on the ROC curve, which maximized the overall classification accuracy for the prediction models. This allowed us to assess the sensitivity and specificity of the models at the selected threshold, providing valuable insights into their discriminative ability for lesion malignancy status. For each individual predictive model, we evaluated its performance on the test set by estimating various measures, including the AUC accompanied by its corresponding 95% confidence interval (CI), specificity, and sensitivity. To compare the performance of different models, we conducted pair-wise comparisons based on the AUC using DeLong's test for paired data. Hypothesis testing was performed with a two-sided alternative whenever appropriate, and the significance level was set at $\alpha = 0.05$, indicating a 5% probability of a Type I error. All reported p-values are unadjusted for multiple testing, and all statistical analyses were performed using RStudio (R version 4.2.3; R Core Team, Vienna, Austria).

RESULTS

A total of 85 female patients (mean age, 57 years ± 13) with 85 suspicious ALNs were included in the analysis. The histopathology results of FNAB confirmed of 42 metastatic and 43 reactive lymph nodes. Patients' ages ranged from 28 to 88 years (mean±standard deviation: 56±13) in the metastatic group, and 28 to 79 years (mean±standard deviation: 58±14) in the reactive group. The size of the lymph nodes ranged from 5.5 mm to 30.5 mm for the metastatic group and 6 mm to 30.4 mm for the reactive group. Cortical thickness ranged from 2.5 mm to 25 mm in the metastatic group and 1.4 mm to 10.6 mm in the reactive group.

Of the 85 patients included in the study, 82 had breast cancer as the primary malignancy. Among the remaining three patients, one patient with metastatic lymph node had chronic lymphocytic leukemia, and in two reactive ALN patients, no cancer was detected. Table 1 provides a summary of the clinical characteristics of the participants, along with the corresponding qHDMI, biomarkers, SWE metrics, and their respective p-values.

Table 1 Patients' age, node characteristics, and summary of SWE and HDMI quantitative parameters.

	Reactive[(a)] N=42	Metastatic[(a)] N=43	P-value[(b)]
Clinical			
Age	58 ± 14	56 ± 13	0.40
Node size(mm)	14 ± 5.70	17 ± 6.50	**0.01**
Cortical thickness(mm)	4.10 ± 1.70	7.30 ± 4.10	**<0.0001**
qHDMI biomarkers			
τ_{mean}	1.00 ± 0.03	1 ± 0.02	**0.002**
τ_{max}	1.10 ± 0.16	1.20 ± 0.18	**<0.0001**
NV	5.80 ± 7	16 ± 15	**<0.0001**
NB	2.60 ± 3.70	8.00 ± 9.60	**0.0004**
VD	0.03 ± 0.03	0.05 ± 0.04	**0.01**
FD	1.00 ± 0.28	1.20 ± 0.29	**0.0003**
D_{max}	630 ± 188	795 ± 168	**0.0001**
D_{mean}	425 ± 125	445 ± 72	0.2
MD_{max}	0.26 ± 0.33	0.50 ± 0.30	**0.001**
BA_{max}	56 ± 64	96 ± 59	**0.007**
SWE metrics			
E_{mean}	17 ± 10	44 ± 23	**<0.0001**
E_{max}	42 ± 28	116 ± 48	**<0.0001**
f_{mass}	175 ± 81	241 ± 126	**0.007**

(a) Values are presented as mean ± standard deviation, (b) P-values in bold indicate statistical significance (values less 0.05)

The visual representation of the HDMI and SWE images and their corresponding B-mode ultrasound of a metastatic and a reactive ALN, along with the values of respective qHDMI biomarkers and SWE metrics, are displayed in Fig. 1. Fig. 1 (top row) shows the HDMI and SWE images of a metastatic lymph node from a woman in her 60s with grade II invasive lobular carcinoma. B-mode ultrasound image shows a large lymph node, 30 mm in largest dimension with a cortical thickness of 12.2 mm. Fig. 1 (bottom row) shows the HDMI and SWE images of a reactive lymph node in a woman in her 60s with grade 3 invasive

ductal carcinoma with the corresponding qHDMI biomarkers and SWE metrics. The ultrasound features include a node size of 11.5 mm in the largest dimension with a cortical thickness of 4 mm. The hypervascularity and morphological vessel irregularity, along with the associated qHDMI biomarkers and SWE metrics, suggest this ALN is metastatic.

The distributions of all the 10 qHDMI and three SWE metrics for the metastatic and reactive ALNs are depicted in Fig. 3. SWE values (E_{mean}, E_{max}, f_{mass}) were notably higher in the metastatic group. Furthermore, qHDMI biomarkers, including FD, NB, NV, VD, $D_{max,}$ τ_{max}, τ_{mean}, MD_{max}, and BA_{max}, were significantly higher in the metastatic nodes.

Fig.2 illustrates the Spearmean correlation coefficient between the significant SWE and qHDMI measures. All coefficients fall below 0.40 indicating low correlation among biomarkers of these two different methods.

Classification models

In our study, five distinct models (SWE, qHDMI, qHDMI-SWE, qHDMI-SWE-C, and Clinical) were trained and employed to classify malignant and benign ALNs, yielding the following outcomes: The SWE model demonstrated a sensitivity of 0.93, and a specificity of 0.91 with an AUC of 0.93. The qHDMI model, trained on the significant qHDMI parameters (NV, NB, VD, D_{max}, τ_{mean}, τ_{max}, BA_{max}, MD_{max}, and FD), exhibited a sensitivity of 0.87, a specificity of 1.00, and an AUC of 0.97. The sensitivity and specificity of the qHDMI-SWE model were found to be 0.93 and 1.00, respectively, with an AUC of 0.97. The qHDMI-SWE-C model integrated qHDMI, SWE, and clinical parameters. This model displayed a sensitivity of 0.87, a specificity of 1.00, and an AUC of 0.98. Finally, the Clinical model, trained only on age, maximum diameter of ALN, and ALN cortical thickness, achieved a sensitivity of 40% and a specificity of 91%, with an AUC of 0.62. Fig. 4 demonstrates all models' ROC curves, and the table beneath the plots contains performance metrics of the models.

Table 2 shows the pair-wise AUC comparisons between the five developed models using the p-values obtained from the DeLong's test. The results indicate that compared to the baseline Clinical model, all the models exhibit improved classification performance. On the other hand, even though the qHDMI model had higher AUC than the SWE model (0.97 compared to 0.93), and the addition of clinical features to the combination of SWE and qHDMI biomarkers led to a slight increase in the AUC (up to 0.98), these improvements were not statistically significant.

Table 2: P-values of AUC pair-wise comparisons using DeLong test.

Model (AUC)	Clinical (0.62)	SWE (0.93)	qHDMI (0.97)	qHDMI-SWE (0.97)	qHDMI-SWE-C (0.98)
Clinical (0.62)	1.0000	**0.0100**	**0.0011**	**0.0017**	**0.0007**
SWE (0.93)	**0.0100**	1.0000	0.5780	0.2044	0.3110
qHDMI (0.97)	**0.0011**	0.5780	1.0000	0.8754	0.6619
qHDMI-SWE (0.97)	**0.0017**	0.2044	0.8754	1.0000	0.7314
qHDMI-SWE-C (0.98)	**0.0007**	0.3110	0.6619	0.7314	1.0000

P-values in bold indicate statistical significance (values less 0.05)

The visual representation and quantitative measures of the qHDMI and SWE images for a metastatic and a reactive ALN with false negative and false positive SWE outcomes are displayed in Fig. 5. The qHDMI and SWE images of a metastatic lymph node from a woman in her 60s with grade II invasive ductal carcinoma are shown in Fig. 5, top row. B-mode ultrasound image of this node shows a lymph node of 5.5 mm in largest dimension with a cortical thickness of 3.6 mm. While visual presentation and quantitative biomarkers of qHDMI suggest this ALN as metastatic, the SWE map and estimates incorrectly favored this ALN as reactive. Furthermore, the HDMI images and quantitative biomarkers of a reactive lymph node with a size of 10 mm in largest dimension and with a cortical thickness of 4.1 mm, from a woman in her 50s with grade II invasive ductal carcinoma suggest a reactive ALN, but the SWE map estimating high stiffness falsely suggests a metastatic ALN (Fig. 5, bottom row).

Breast cancer subtypes

In this study, we also conducted an analysis to investigate associations between breast cancer immunohistochemical subtypes luminal A and B and qHDMI and SWE biomarkers of ALNs. Specifically, we investigated distributional differences of the qHDMI and SWE biomarkers between ALNs with these two subtypes as the primary cancer. Among our 81 breast cancer patients, we could gather immunohistochemical data from 67 patients. 21 patients were Luminal A, 41 were Luminal B, 2 were HER2+, and three were triple-negative (TNBC). Since luminal A and B comprised most of the sample, we did the analysis only for the comparison of the luminal A and B groups.

Fig. 6 offers an overview of the set of biomarkers that displayed statistically significant distributional differences for the two different luminal subtypes, identified using the Wilcoxon rank-sum test. The more aggressive luminal subtype B corresponded to higher elasticity values (E_{max} and E_{mean}) and qHDMI biomarkers (NV, MD_{max}, τ_{max}, and FD).

DISCUSSION

In this study, we compared the effectiveness of two ultrasound methodologies, quantitative HDMI and SWE, as well as combining the quantitative parameters of these two imaging tools in differentiating metastatic and reactive ALNs. Additionally, we sought the effect of adding clinical factors to the combined model. The results of this study showed that qHDMI prediction model biomarkers can determine the status of ALNs with high accuracy, AUC of 0.97 and accuracy of 0.92. SWE prediction model as well as combining qHDMI biomarkers with those of SWE parameters did not exhibit statistically significant differences in terms of the accuracy in differentiating metastatic and reactive ALNs. Therefore, our findings underscore the potential effectiveness of qHDMI biomarkers in determining the status of suspicious ALNs, which is in agreement with the results of the previous study [24]. On the other end of the spectrum, the Clinical predictive model demonstrated an AUC of 0.62, which was much lower than the performance achieved by other individual predictive models, qHDMI and SWE, developed in this study. As shown in Fig. 2, there are very low correlation between the SWE and qHDMI measures indicating that these two sets of parameters are independent from each other.

In another study, the authors used the two independent quantitative parameters, SWE estimating tumor stiffness and qHDMI biomarkers quantifying tumor angiogenesis for the differentiation of benign and malignant breast lesions. However, unlike the findings of the present study on predicting metastasis, the authors demonstrated a significant improvement of using combined qHDMI-SWE over the individual SWE or qHDMI models for the differentiation of benign and malignant breast lesions [38].

Previous studies have reported SWE estimation to be helpful in distinguishing between reactive and metastatic axillary lymph nodes with various accuracies [16, 39, 40]. Similar to the current study, Gregory et al. demonstrated high sensitivity and specificity for differentiation of reactive and metastatic ALNs using quantitative SWE [17].

The potential of qHDMI biomarkers in differentiating metastatic and reactive axillary lymph nodes was previously investigated, and the predictive models trained on HDMI biomarkers were shown to be capable of ALN characterization with high accuracy, highlighting the utility of qHDMI-based biomarkers [24]. Superb microvascular imaging (SMI) and power Doppler US have been used to differentiate metastatic from reactive ALNs; however, the quantitative analysis was limited to counting vascular branches [25]. Moreover, another study found a better diagnostic performance of SMI compared to SWE in differentiating metastatic ALN from lymphadenitis [41]. However, quantitative analysis for SMI in this study was limited to the vascularity index, while in our study, a number of quantitative HDMI biomarkers based on morphological features of microvessels are used for classification.

Significant associations were identified between breast cancer subtypes Luminal A and B and the evaluated parameters, including elasticity parameters (E_{max} and E_{mean}) and qHDMI biomarkers (NV, MD_{max}, τ_{max}, and FD). Consistent with our study, Gu et al. demonstrated a relationship between higher E_{max} and E_{mean} values with poor prognosis [32].

This study has some limitations. First, it was a single-center study with a limited number of participants. Future direction involves conducting the study on a larger population of breast cancer patients to increase precision in model performance estimation and pair-wise comparisons. Moreover, our study primarily relied on 2D microvasculature imaging. The implementation of our newly developed 3D qHDMI [42] and ongoing research would be helpful in overcoming this limitation. Furthermore, a future multicenter comprehensive study will determine the capability of the ultrasound-based quantitative microvessel imaging for the characterization of ALNs in large numbers of diverse patients with all challenging situations, as well as breast cancer patients with ALN metastasis who undergo neoadjuvant therapy.

Conclusion

In summary, our study compares the effectiveness of quantitative biomarkers of qHDMI, SWE estimates and combining the two, SWE and qHDMI for improved characterization of axillary lymph nodes. The results conclude that HDMI-prediction model was able to separate metastatic from reactive ALNs with high accuracy. Compared to a baseline Clinical model, models trained on qHDMI, SWE, and the combined models showed enhanced classification accuracy. The qHDMI biomarkers can be valuable in determining the status of suspicious ALNs, providing helpful information regarding breast cancer prognosis.

Declarations

Data availability

The data that support the findings of this study are available from the corresponding author upon reasonable request. The requested data may include figures that have associated raw data. Because the study was conducted on human volunteers, the release of patient data may be restricted by Mayo policy and needs special request. The request can be sent to: Karen A. Hartman, MSN, CHRC | Administrator - Research Compliance| Integrity and Compliance Office | Assistant Professor of Health Care Administration, Mayo Clinic College of Medicine & Science | 507-538-5238 | Administrative Assistant: 507-266-6286 | hartman.karen@mayo.edu Mayo Clinic | 200 First Street SW | Rochester, MN 55905 | mayoclinic.org.

We do not have publicly available Accession codes, unique identifiers, or web links.

CODE AVAILABLITY

The custom code or mathematical algorithms that are deemed central to the conclusions are available from the corresponding author upon request.

Acknowledgments

Financial Support: This work was supported in part by the NIH Grants R01CA239548 (A. Alizad and M. Fatemi) and R01CA195527 (M. Fatemi and A. Alizad). The content is solely the responsibility of the authors and does not necessarily represent the official views of NIH. The NIH did not have any additional role in the study design, data collection and analysis, decision to publish or preparation of the manuscript.

Author Contributions:

Conceptualization and design: A. Alizad, M. Fatemi

Methodology: A. Alizad, M. Fatemi

Investigation: A. Alizad, M. Fatemi

Software: S. Sabeti

Data curation: S. Sabeti S., Sotoudehnia

Visualization: S. Sabeti, A. Alizad, M. Fatemi, S. Sotoudehnia, D.P. Rosen

Validation: A. Alizad, M. Fatemi, S. Sabeti, N.B. Larson, R.T. Fazzio

Formal analysis (e.g., statistical analysis, biostatistics, computational analysis): S. Sotoudehnia, S. Sabeti, N.B. Larson, D.P. Rosen

Writing-original draft: A. Alizad, S. Sabeti, S. Sotoudehnia,

Writing, review and edits: A. Alizad, M. Fatemi, N.B. Larson, S. Sabeti, R.T. Fazzio, S. Sotoudehnia, D.P. Rosen

Administrative, Resources: A. Alizad, M. Fatemi

Funding acquisition: A. Alizad, M. Fatemi

Study supervision: A. Alizad, M. Fatemi

Conflict of interest statement

The authors of this manuscript declare no relationships with any companies, whose products or services may be related to the subject matter of the article, and the authors affirm that they do not have any potential financial interest related to the technology referenced in this paper.

Ethical Approval

The Research involved human participants. The study was approved by Institutional Review Board (IRB) of Mayo Clinic (IRB # 13-006035, last approval date: 6/1/2023 and IRB # 19-003028, last

approved 3/22/2023) and was Health Insurance Portability and Accountability Act compliant. All procedures performed in this study were in accordance with the ethical standards of the institutional and/or national research committee and with the 1964 Helsinki declaration and its later amendments or comparable ethical standards.

Informed Consent Statement: Signed IRB approved informed consent with permission for publication was obtained from all individual participants included in the study.

Financial Support: This work was supported in part by the NIH Grants R01CA239548 and R01CA195527 (A. Alizad and M. Fatemi).

References

1. Chang JM, Leung JWT, Moy L, Ha SM, Moon WK: Axillary Nodal Evaluation in Breast Cancer: State of the Art. Radiology 2020, 295(3):500–515.
2. Majid S, Tengrup I, Manjer J: Clinical assessment of axillary lymph nodes and tumor size in breast cancer compared with histopathological examination: a population-based analysis of 2,537 women. World J Surg 2013, 37(1):67–71.
3. Chung HL, Le-Petross HT, Leung JWT: Imaging Updates to Breast Cancer Lymph Node Management. Radiographics 2021, 41(5):1283–1299.
4. Alvarez S, Añorbe E, Alcorta P, López F, Alonso I, Cortés J: Role of sonography in the diagnosis of axillary lymph node metastases in breast cancer: a systematic review. American Journal of Roentgenology 2006, 186(5):1342–1348.
5. Marino MA, Avendano D, Zapata P, Riedl CC, Pinker K: Lymph node imaging in patients with primary breast cancer: concurrent diagnostic tools. The oncologist 2020, 25(2):e231-e242.
6. Lanng C, Hoffmann J, Galatius H, Engel U: Assessment of clinical palpation of the axilla as a criterion for performing the sentinel node procedure in breast cancer. European Journal of Surgical Oncology (EJSO) 2007, 33(3):281–284.
7. Mansel RE, Fallowfield L, Kissin M, Goyal A, Newcombe RG, Dixon JM, Yiangou C, Horgan K, Bundred N, Monypenny I: Randomized multicenter trial of sentinel node biopsy versus standard axillary treatment in operable breast cancer: the ALMANAC Trial. Journal of the National Cancer Institute 2006, 98(9):599–609.
8. Krag DN, Anderson SJ, Julian TB, Brown AM, Harlow SP, Costantino JP, Ashikaga T, Weaver DL, Mamounas EP, Jalovec LM: Sentinel-lymph-node resection compared with conventional axillary-lymph-node dissection in clinically node-negative patients with breast cancer: overall survival findings from the NSABP B-32 randomised phase 3 trial. The lancet oncology 2010, 11(10):927–933.
9. Alkuwari E, Auger M: Accuracy of fine-needle aspiration cytology of axillary lymph nodes in breast cancer patients: a study of 115 cases with cytologic-histologic correlation. Cancer Cytopathology: Interdisciplinary International Journal of the American Cancer Society 2008, 114(2):89–93.

10. Vijayaraghavan GR, Vedantham S, Kataoka M, DeBenedectis C, Quinlan RM: The relevance of ultrasound imaging of suspicious axillary lymph nodes and fine-needle aspiration biopsy in the post-ACOSOG Z11 era in early breast cancer. Academic radiology 2017, 24(3):308–315.
11. Bayat M, Denis M, Gregory A, Mehrmohammadi M, Kumar V, Meixner D, Fazzio RT, Fatemi M, Alizad A: Diagnostic features of quantitative comb-push shear elastography for breast lesion differentiation. PloS one 2017, 12(3):e0172801.
12. Denis M, Bayat M, Mehrmohammadi M, Gregory A, Song P, Whaley DH, Pruthi S, Chen S, Fatemi M, Alizad A: Update on breast cancer detection using comb-push ultrasound shear elastography. IEEE transactions on ultrasonics, ferroelectrics, and frequency control 2015, 62(9):1644–1650.
13. Berg WA, Cosgrove DO, Doré CJ, Schäfer FK, Svensson WE, Hooley RJ, Ohlinger R, Mendelson EB, Balu-Maestro C, Locatelli M: Shear-wave elastography improves the specificity of breast US: the BE1 multinational study of 939 masses. Radiology 2012, 262(2):435–449.
14. Cosgrove DO, Berg WA, Doré CJ, Skyba DM, Henry J-P, Gay J, Cohen-Bacrie C, Group BS: Shear wave elastography for breast masses is highly reproducible. European radiology 2012, 22:1023–1032.
15. Gu J, Polley EC, Ternifi R, Nayak R, Boughey JC, Fazzio RT, Fatemi M, Alizad A: Individualized-thresholding Shear Wave Elastography combined with clinical factors improves specificity in discriminating breast masses. The breast 2020, 54:248–255.
16. Ng WL, Omar N, Ab Mumin N, Hamid MTR, Vijayananthan A, Rahmat K: Diagnostic accuracy of shear wave elastography as an adjunct tool in detecting axillary lymph nodes metastasis. Academic radiology 2022, 29:S69-S78.
17. Gregory A, Denis M, Bayat M, Kumar V, Kim BH, Webb J, Nayak R, Adabi S, Meixner DD, Polley EC *et al*: Predictive value of comb-push ultrasound shear elastography for the differentiation of reactive and metastatic axillary lymph nodes: A preliminary investigation. PLoS One 2020, 15(1):e0226994.
18. Evans A, Rauchhaus P, Whelehan P, Thomson K, Purdie CA, Jordan LB, Michie CO, Thompson A, Vinnicombe S: Does shear wave ultrasound independently predict axillary lymph node metastasis in women with invasive breast cancer? Breast cancer research and treatment 2014, 143:153–157.
19. Lee E, Koskimaki JE, Pandey NB, Popel AS: Inhibition of lymphangiogenesis and angiogenesis in breast tumor xenografts and lymph nodes by a peptide derived from transmembrane protein 45A. Neoplasia 2013, 15(2):112-IN116.
20. Longatto Filho A, Lopes JM, Schmitt FC: Angiogenesis and breast cancer. *Journal of oncology* 2010, 2010.
21. Nakamura Y, Yasuoka H, Tsujimoto M, Yang Q, Imabun S, Nakahara M, Nakao K, Nakamura M, Mori I, Kakudo K: Flt-4-positive vessel density correlates with vascular endothelial growth factor-d expression, nodal status, and prognosis in breast cancer. Clinical Cancer Research 2003, 9(14):5313–5317.
22. Nagy J, Chang SH, Dvorak AM, Dvorak HF: Why are tumour blood vessels abnormal and why is it important to know? British journal of cancer 2009, 100(6):865–869.

23. Guidi AJ, Berry DA, Broadwater G, Perloff M, Norton L, Barcos MP, Hayes DF: Association of angiogenesis in lymph node metastases with outcome of breast cancer. Journal of the National Cancer Institute 2000, 92(6):486–492.
24. Ferroni G, Sabeti S, Abdus-Shakur T, Scalise L, Carter JM, Fazzio RT, Larson NB, Fatemi M, Alizad A: Noninvasive prediction of axillary lymph node breast cancer metastasis using morphometric analysis of nodal tumor microvessels in a contrast-free ultrasound approach. Breast Cancer Research 2023, 25(1):65.
25. Kurt SA, Eryurekli AE, Kayadibi Y, Samanci C, Velidedeoglu M, Onur I, Arslan S, Taskin F: Diagnostic performance of superb microvascular imaging in differentiating benign and malignant axillary lymph nodes. Ultrasound Quarterly 2023, 39(2):74–80.
26. Bayat M, Fatemi M, Alizad A: Background removal and vessel filtering of noncontrast ultrasound images of microvasculature. IEEE Transactions on Biomedical Engineering 2018, 66(3):831–842.
27. Ghavami S, Bayat M, Fatemi M, Alizad A: Quantification of morphological features in non-contrast-enhanced ultrasound microvasculature imaging. IEEE Access 2020, 8:18925–18937.
28. Ternifi R, Wang Y, Polley EC, Fazzio RT, Fatemi M, Alizad A: Quantitative biomarkers for cancer detection using contrast-free ultrasound high-definition microvessel imaging: fractal dimension, Murray's deviation, bifurcation angle & spatial vascularity pattern. IEEE transactions on medical imaging 2021, 40(12):3891–3900.
29. Ternifi R, Wang Y, Gu J, Polley EC, Carter JM, Pruthi S, Boughey JC, Fazzio RT, Fatemi M, Alizad A: Ultrasound high-definition microvasculature imaging with novel quantitative biomarkers improves breast cancer detection accuracy. European Radiology 2022, 32(11):7448–7462.
30. Kurti M, Sabeti S, Robinson KA, Scalise L, Larson NB, Fatemi M, Alizad A: Quantitative Biomarkers Derived from a Novel Contrast-Free Ultrasound High-Definition Microvessel Imaging for Distinguishing Thyroid Nodules. Cancers 2023, 15(6):1888.
31. Sabeti S, Ternifi R, Larson NB, Olson MC, Atwell TD, Fatemi M, Alizad A: Morphometric analysis of tumor microvessels for detection of hepatocellular carcinoma using contrast-free ultrasound imaging: A feasibility study. Frontiers in Oncology 2023, 13.
32. Gu J, Polley EC, Boughey JC, Fazzio RT, Fatemi M, Alizad A: Prediction of invasive breast cancer using mass characteristic frequency and elasticity in correlation with prognostic histologic features and immunohistochemical biomarkers. Ultrasound in medicine & biology 2021, 47(8):2193–2201.
33. Gu J, Polley EC, Denis M, Carter JM, Pruthi S, Gregory AV, Boughey JC, Fazzio RT, Fatemi M, Alizad A: Early assessment of shear wave elastography parameters foresees the response to neoadjuvant chemotherapy in patients with invasive breast cancer. Breast Cancer Research 2021, 23(1):52.
34. Nayak R, Fatemi M, Alizad A: Adaptive background noise bias suppression in contrast-free ultrasound microvascular imaging. Physics in Medicine & Biology 2019, 64(24):245015.
35. Nayak R, Kumar V, Webb J, Gregory A, Fatemi M, Alizad A: Non-contrast agent based small vessel imaging of human thyroid using motion corrected power Doppler imaging. Scientific Reports 2018, 8(1):15318.

36. Nayak R, MacNeill J, Flores C, Webb J, Fatemi M, Alizad A: Quantitative assessment of ensemble coherency in contrast-free ultrasound microvasculature imaging. Medical physics 2021, 48(7):3540–3558.
37. Fluss R, Faraggi D, Reiser B: Estimation of the Youden Index and its associated cutoff point. Biometrical Journal: Journal of Mathematical Methods in Biosciences 2005, 47(4):458–472.
38. Gu J, Ternifi R, Larson NB, Carter JM, Boughey JC, Stan DL, Fazzio RT, Fatemi M, Alizad A: Hybrid high-definition microvessel imaging/shear wave elastography improves breast lesion characterization. Breast Cancer Res 2022, 24(1):16.
39. Cheng Y, Li G, Jing H, Yuan S, Zhang L, Cheng W: Effectiveness of quantitative shear wave elastography for the prediction of axillary lymph node metastasis. *Evidence-Based Complementary and Alternative Medicine* 2022, 2022.
40. Youk JH, Son EJ, Kim J-A, Gweon HM: Pre-operative evaluation of axillary lymph node status in patients with suspected breast cancer using shear wave elastography. Ultrasound in medicine & biology 2017, 43(8):1581–1586.
41. Uslu H, Tosun M: The benefit of superb microvascular imaging and shear wave elastography in differentiating metastatic axillary lymphadenopathy from lymphadenitis. Clinical Breast Cancer 2022, 22(6):515–520.
42. Gu J, Ternifi R, Sabeti S, Larson NB, Carter JM, Fazzio RT, Fatemi M, Alizad A: Volumetric imaging and morphometric analysis of breast tumor angiogenesis using a new contrast-free ultrasound technique: a feasibility study. Breast Cancer Research 2022, 24(1):85.

Figures

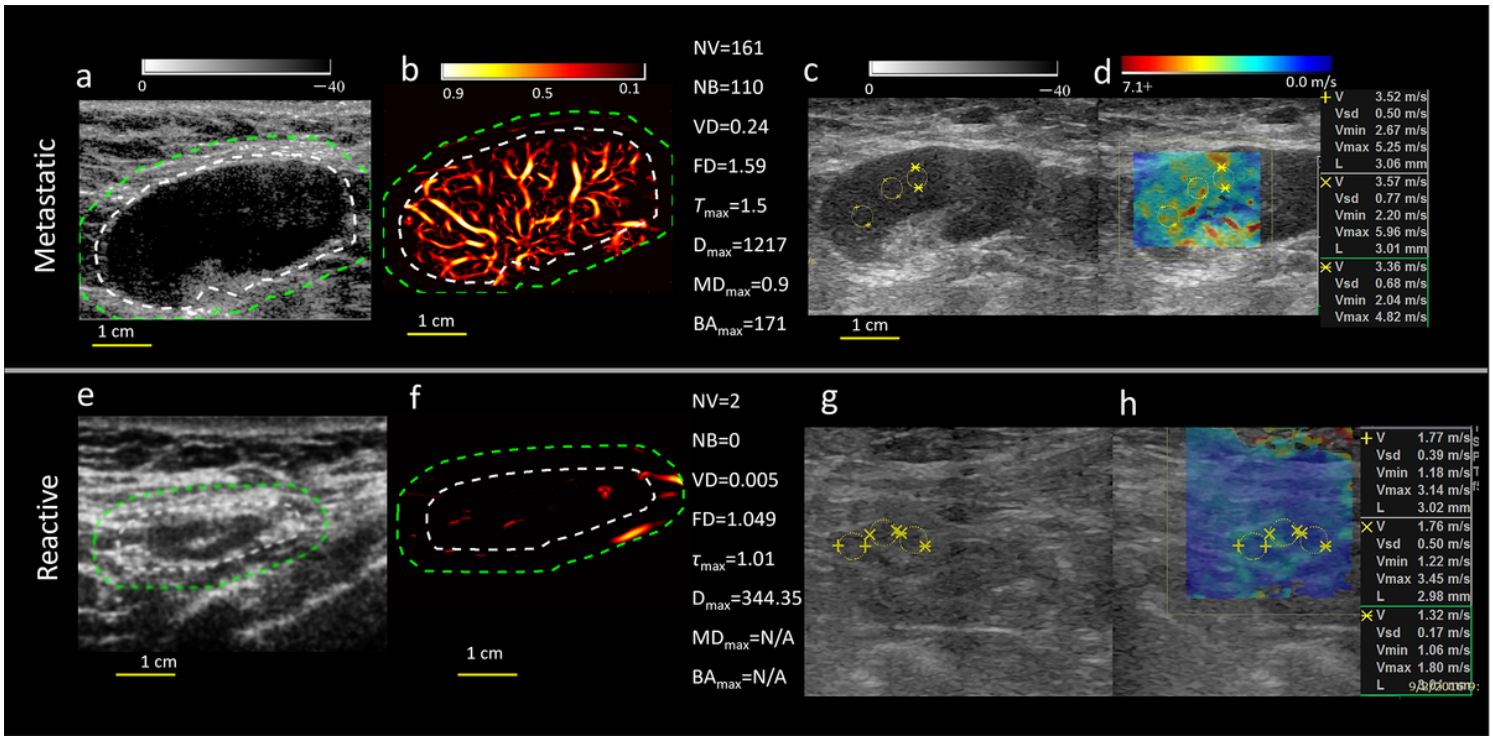

Figure 1

B-mode images (a, e), HDMI images (b, f), and SWE B-mode and elasticity maps (c, g and d, h) of a metastatic (top) and a reactive (bottom) ALNs. In B-mode and HDMI images, white dashed lines indicate the boundaries of the lymph node, and green dashed lines depict these boundaries after a 2 mm dilation. Selected qHDMI biomarkers and SWE metrics are presented to the right of the corresponding images.

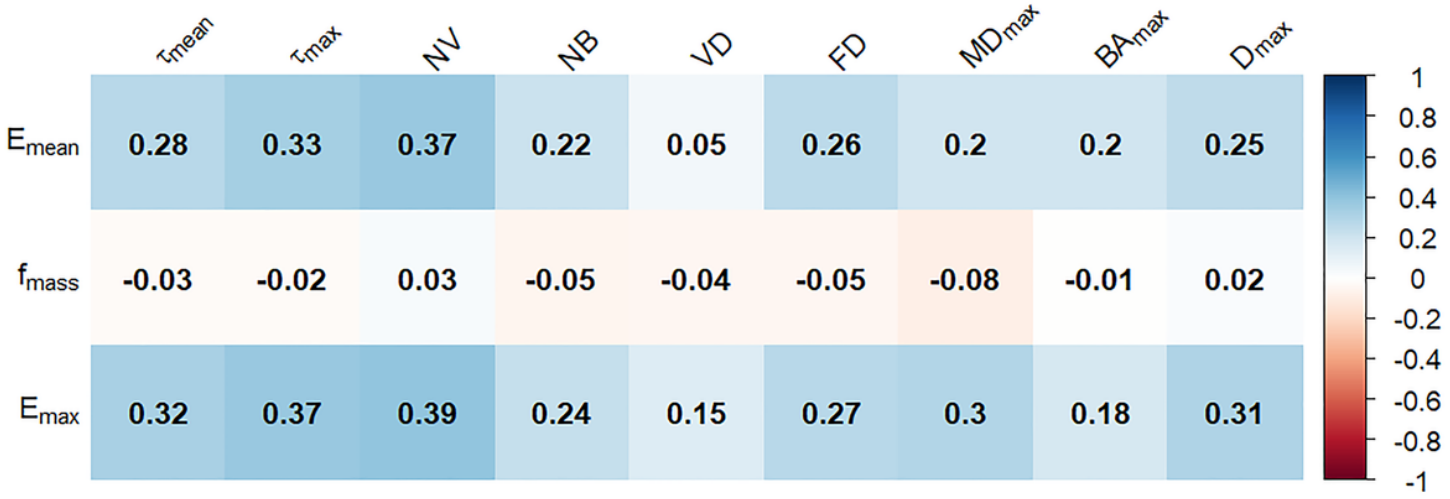

Figure 2

Spearman correlation coefficient plot between SWE and qHDMI biomarkers

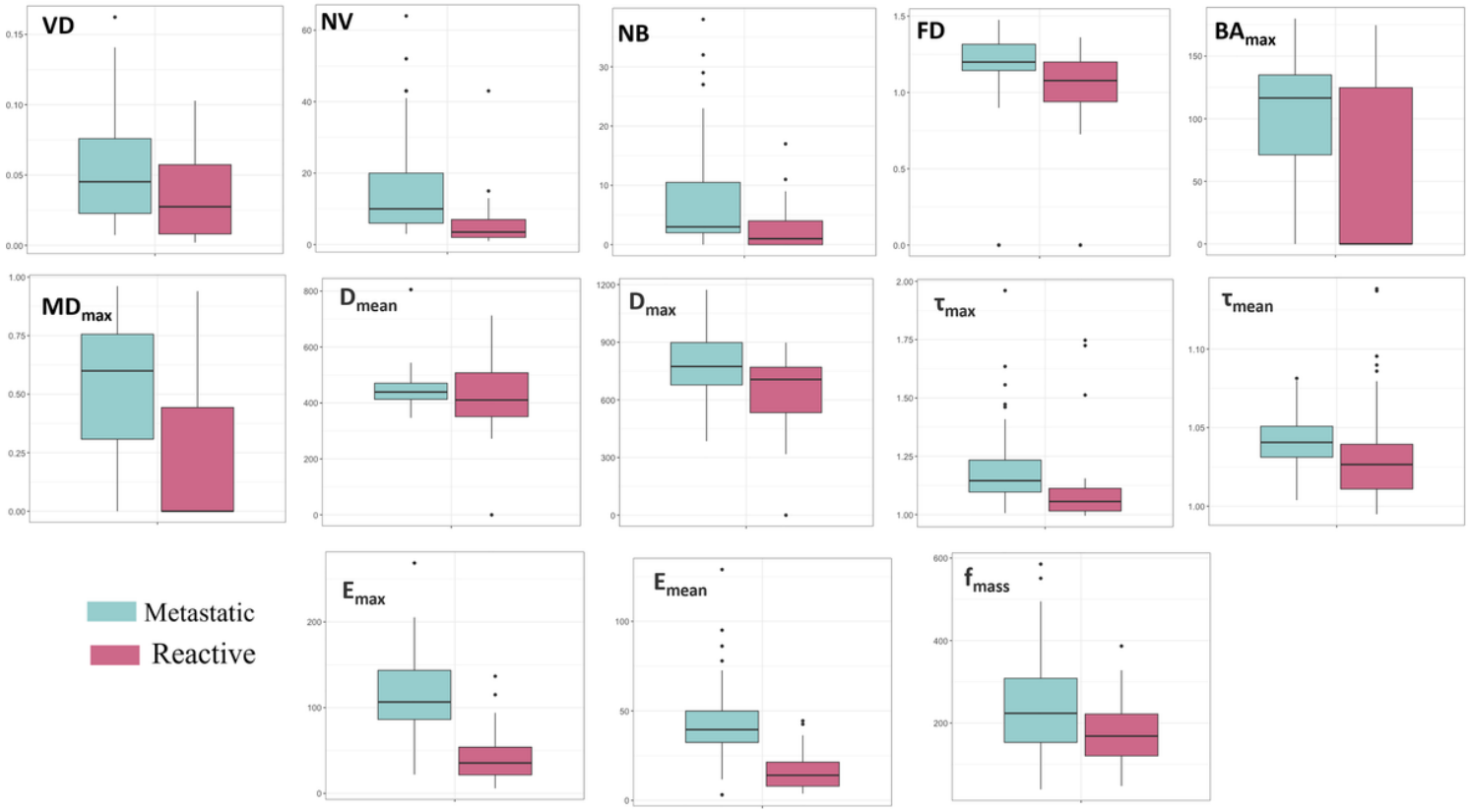

Figure 3

Box plots of quantitative HDMI and SWE biomarkers for the metastatic (cyan) and reactive (magenta) lymph nodes.

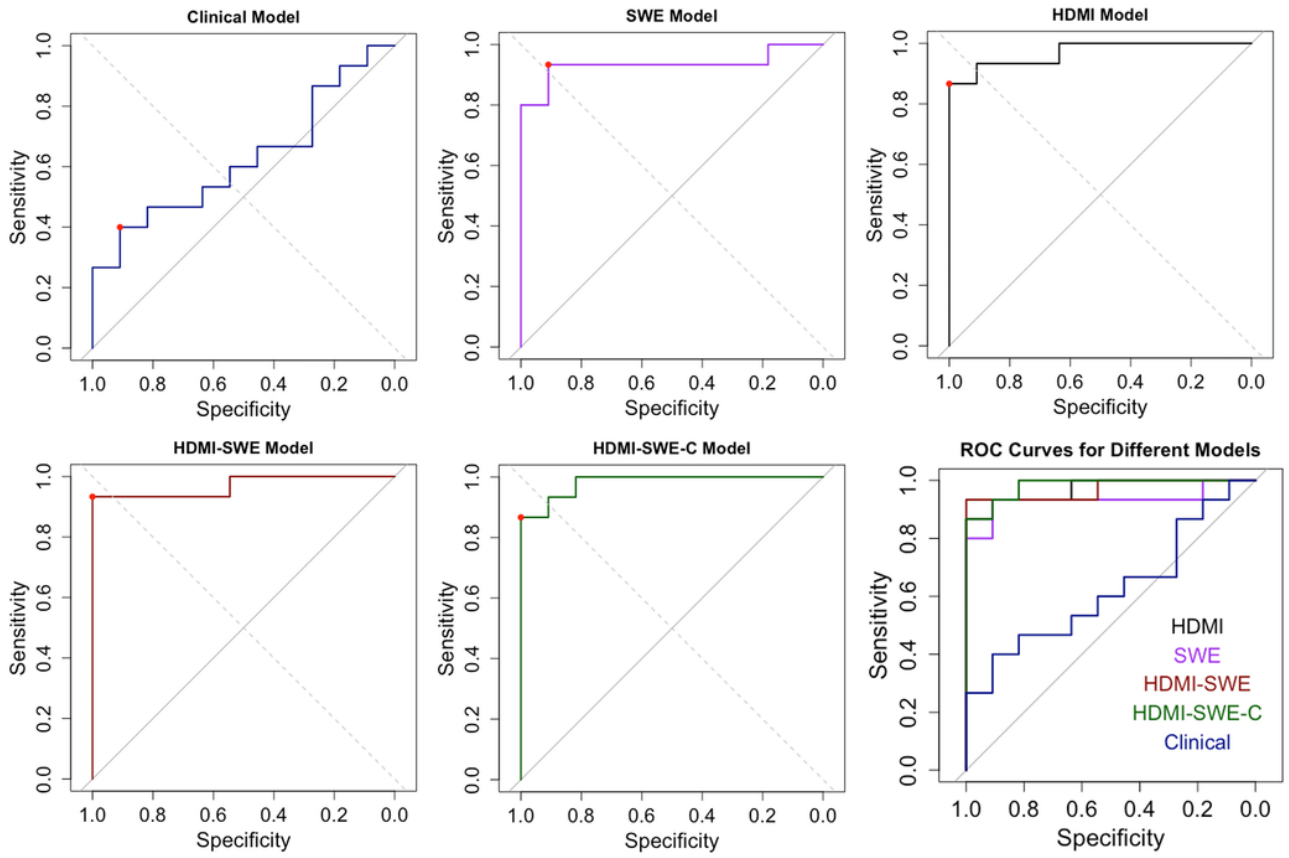

Prediction models	AUC	95%CI	Cutoff	Sensitivity	Specificity	Precision	Accuracy	FP	FN	TP	TN
1-Clinical	0.62	[0.39,0.84]	0.56	0.40	0.91	0.86	0.61	1	9	6	10
2-SWE	0.93	[0.82,1.00]	0.20	0.93	0.91	0.91	0.92	1	1	14	10
3-HDMI	0.97	[0.91,1.00]	0.47	0.87	1.00	1.00	0.92	0	2	13	11
4-HDMI-SWE	0.97	[0.92,1.00]	0.26	0.93	1.00	0.96	0.92	0	1	14	11
5-HDMI-SWE-C	0.98	[0.94,1.00]	0.48	0.87	1.00	1.00	0.92	0	2	13	11

Figure 4

ROC curves for all the models and the table containing performance metrics of the models. FP (False positive), FN (False negative), TP (True positive), TN (True Negative).

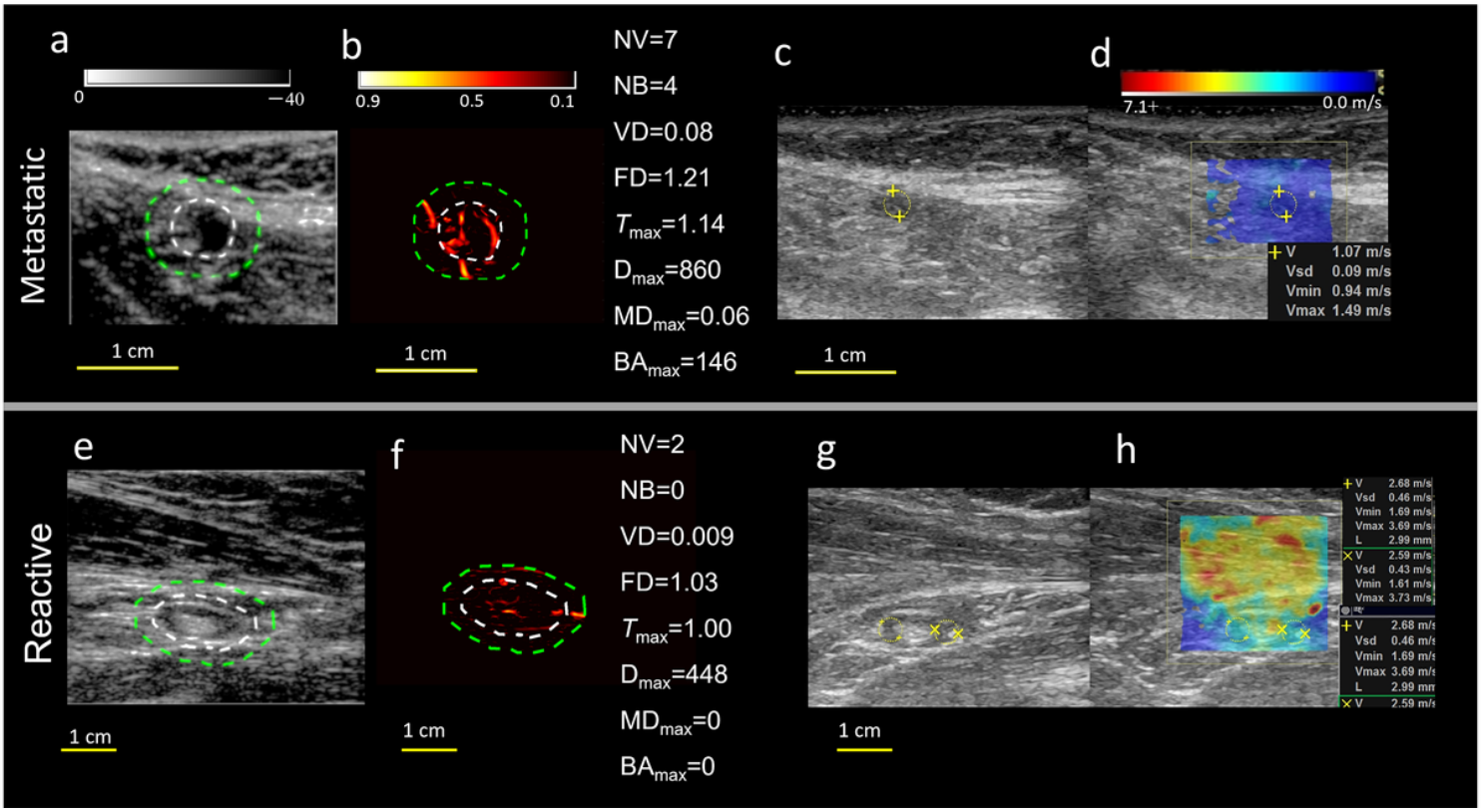

Figure 5

B-mode images (a, e), HDMI images (b, f), and SWE B-mode and elasticity maps (c, g and d, h) of a metastatic (top) and a reactive (bottom) ALNs. In B-mode and HDMI images, white dashed lines indicate the boundaries of the node, and green dashed lines depict these boundaries after a 2 mm dilation. Selected qHDMI biomarkers and SWE metrics are presented to the right of the corresponding images. Figures at the top and bottom present cases where the SWE model (in contrast to the qHDMI model) had a false negative and a false positive, respectively.

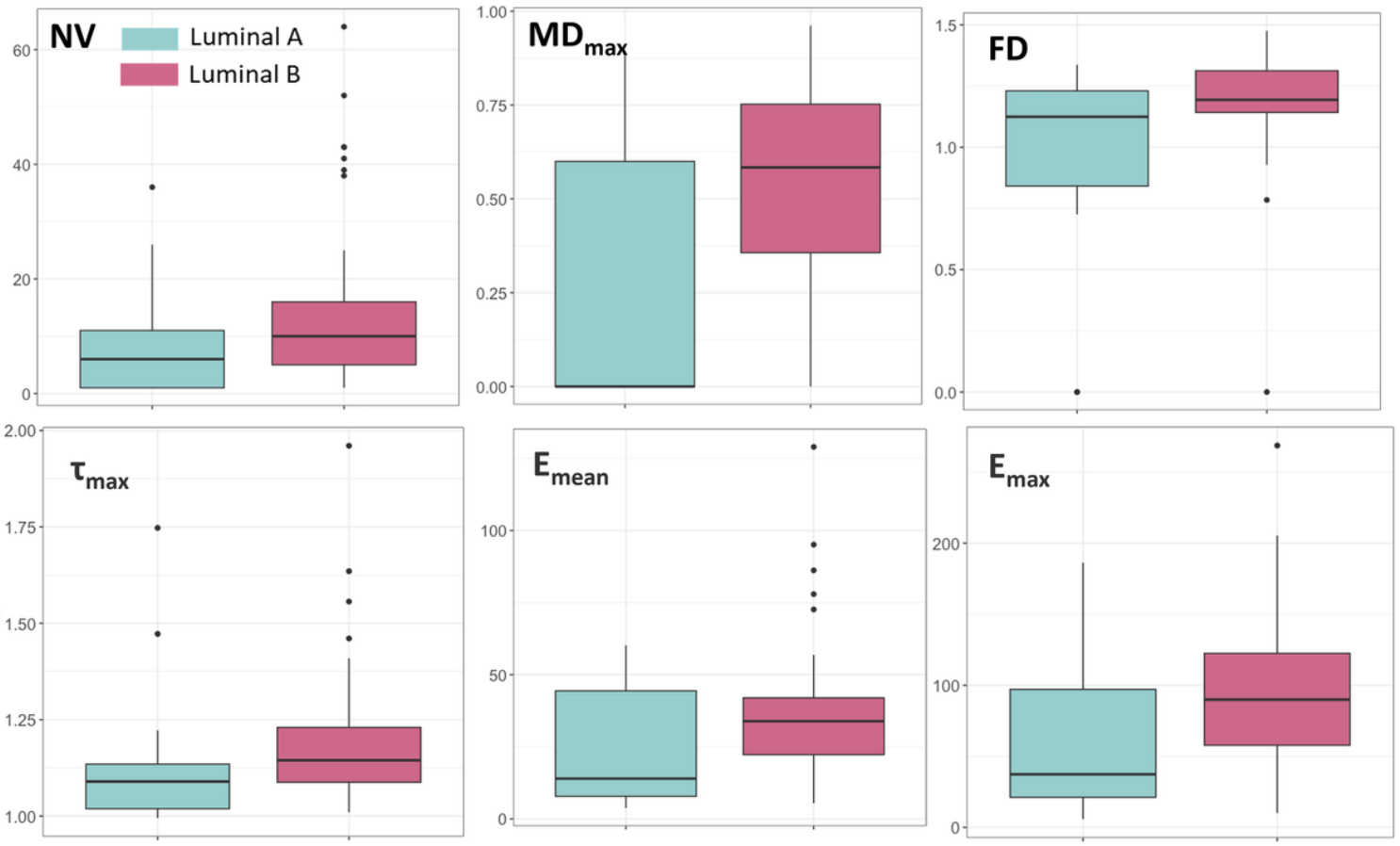

	Luminal A N=21	Luminal B N=41	P value
HDMI			
NV	8.2 ± 8.8	15 ± 16	**0.04**
MD_{max}	0.28± 0.34	0.51±0.29	**0.01**
FD	0.98 ± 0.37	1.2 ± 0.24	**0.01**
τ_{max}	1.10 ± 0.18	1.2 ± 0.18	**0.02**
SWE			
E_{max}	61 ± 53	98 ± 58	**0.009**
E_{mean}	23 ± 19	38 ± 25	**0.01**

Figure 6

Box plots of qHDMI and SWE biomarkers exhibiting significant distributional differences between ALNs with luminal A (cyan) and luminal B (magenta) breast cancer subtypes as the primary malignancy. The table shows the mean±standard deviation of the biomarker values for the two groups and their corresponding Wilcoxon rank-sum test p-values.